Heliyon 9 (2023) e15919

Contents lists available at ScienceDirect

Heliyon

journal homepage: www.cell.com/heliyon

Research article

Biologically-induced synthetic manganese carbonate precipitate (BISMCP) for potential applications in heavy metal removal

Anggraeni Kumala Dewi [a,b], Raju Kumar Sharma [b,c], Koyeli Das [b,d], Uttara Sukul [b,d], Pin-Yun Lin [c], Yi-Hsun Huang [b], Chung Ming Lu [b,e], Cheng-Kang Lu [f,**], Tsung-Hsien Chen [g], Chien-Yen Chen [b,h,*]

[a] Department of Physics, National Chung Cheng University, University Road, Minhsiung, Chiayi County, 62102, Taiwan
[b] Doctoral Program in Science, Technology, Environment, and Mathematics, Department of Earth and Environmental Sciences, National Chung Cheng University, 168 University Road, Min-Hsiung, Chiayi County, 62102, Taiwan
[c] Department of Chemistry and Biochemistry, National Chung Cheng University, 168 University Road, Min-Hsiung, Chiayi County, 62102, Taiwan
[d] Department of Biomedical Sciences, Graduate Institute of Molecular Biology, National Chung Cheng University, 168 University Road, Min-Hsiung, Chiayi County, 62102, Taiwan
[e] Department of Chemical Engineering, National Chung Cheng University, University Road, Minhsiung, Chiayi County, 62102, Taiwan
[f] Department of Chest Division, Internal Medicine, Ditmanson Medical Foundation Chiayi Christian Hospital 600566, Taiwan
[g] Department of Internal Medicine, Ditmanson Medical Foundation Chiayi Christian Hospital 600566, Taiwan
[h] Center for Nano Bio-Detection, Center for Innovative Research on Aging Society, AIM-HI, National Chung Cheng University, 168, University Road, Min-Hsiung, Chiayi County, 62102, Taiwan

ARTICLE INFO

Keywords:
Adsorbent material
Biologically induced mineralization
Biomineralization
Heavy metal removal
Manganese carbonate ($MnCO_3$)
Sporosarcina pasteurii

ABSTRACT

Heavy metal pollution of water is a burning issue of today's world. Among several strategies involved for heavy metal remediation purpose, biomineralization has shown great potential. Of late, research has been focused on developing effective mineral adsorbents with reduced time and cost consumption. In this present paper, the Biologically-Induced Synthetic Manganese Carbonate Precipitate (BISMCP) was produced based on the biologically-induced mineralization method, employing *Sporosarcina pasteurii* in aqueous solutions containing urea and $MnCl_2$. The prepared adsorbent was characterized using Fourier transform infrared spectroscopy (FTIR), scanning electron microscopy (SEM), SEM-energy dispersive X-ray spectroscopy (SEM-EDX), X-ray diffraction (XRD) and BET surface area analyzer. EDX analysis showed the elements in the crystal BISMCP were Mn, C, and O. XRD result of BISMCP determined the crystal structure, which is close to rhodochrosite ($MnCO_3$). Spectral peaks of FTIR at 1641.79 cm^{-1} confirmed the appearance of C═O binding, with strong stretching of CO_3^{2-} in Amide I. From the six kinds of BISMCP produced, sample MCP-6 has the higher specific surface area by BET analysis at 109.01 m^2/g, with pore size at 8.76 nm and higher pore volume at 0.178 cm^3/g. These specifications will be suitable as an adsorbent for heavy metal removal by adsorption process. This study presents a preliminary analysis of the possibility of BISMCP for heavy metals adsorption using ICP multi-element standard solution XIII (As, Cr, Cd, Cu, Ni, and Zn). BISMCP formed from 0.1 $MnCl_2$ and 30 ml of bacteria volume (MCP-6) produced a better adsorbent material than others concentrations, with

* Corresponding author. Department of Earth and Environmental Sciences, National Chung Cheng University, 168 University Road, Minhsiung, Chiayi County, 62102, Taiwan.
** Corresponding author. Department of Chest Division, Internal Medicine, Ditmanson Medical Foundation Chiayi Christian Hospital, Chiayi City 600566, Taiwan.
E-mail addresses: 07569@cych.org.tw (C.-K. Lu), chien-yen.chen@oriel.oxon.org, yen@eq.ccu.edu.tw (C.-Y. Chen).

https://doi.org/10.1016/j.heliyon.2023.e15919
Received 14 October 2022; Received in revised form 14 January 2023; Accepted 26 April 2023
Available online 1 May 2023

the adsorption efficiency of total As at 98.9%, Cr at 97.0%, Cu at 94.7%, Cd at 88.3%, Zn at 48.6%, and Ni at 29.5%. Future work could be examined its efficiency adsorbing individual heavy metals.

1. Introduction

Heavy metal pollution has become ubiquitous in nature. The hazardous effect of heavy metals can be marked everywhere from the water and soil to the living entity. Being soluble in nature, it causes interference with the human physiological processes which in turn leads to several health disorders. Industrial development is the main cause of this heavy metal pollution; hence attention has been paid to treat this industrial effluent before releasing it into the environment [76]. Numerous methods have been reported to remove heavy metals from the environment, including electrolytic deposition [61], electrochemical [85], ion exchange [64], chemical oxidation-reduction [90], electro-dialysis [39], reverse osmosis [39], membrane separation [70], and solar water evaporation [89]. Instead of having high efficiency these methods are associated with some limitations as well for example high energy consumption, high operation cost, production of toxic sludge etc. The adsorption process is the most commonly used and preferred method for heavy metal removal. This process occurs when the adsorbate is bound to the surface or inside the adsorbent [27]. The adsorption process uses synthetic or natural adsorbents and is simple, cost-effective, and versatile in nature [64,76]. However, recent studies concerned in the development of efficient adsorbent material synthesis, having high-efficiency, high surface area and porosity, but also with reduced synthesis time and cost of adsorbents [34]. Some prominent adsorbents, such as carbon, exhibits great ability for adsorption due to their large surface area and ease of modification with other chemicals. However, the manufacturing cost is high, disposing of activated carbon is difficult, and the regeneration process takes a long time [57,84]. Thus, to overcome these challenges sustainably, green synthesis of mineral is on demand which will serve both the purpose of efficiency as well as cost effectivity.

Biomineralization is one such sustainable approach in which living organisms (bacteria, fungi, algae) combine a number of metal ions (Ca, Fe, Mg, and Mn) with different anions (carbonate, phosphate, oxalate, sulfate, oxides, and sulfides) to produce minerals [9,10,17,35,43,69,71]. The process can further sub-classified into biologically controlled mineralization, biologically influenced mineralization, and biologically induced mineralization [52]. In biologically controlled mineralization, the organism directly affects the nucleation, growth and morphology (such as size, texture and orientation) of the material by controlling the entire biomineralization process through cellular activities [65]. Biologically influenced mineralization is known as passive mineralization, such as mineralization on cell surfaces or mucilaginous or Extracellular Polymeric Substances (EPS) [21]. In biologically induced mineralization, mineral formation occurs when the organisms alter their local micro-environment and foster the extracellular precipitation of mineral phases [54]. This mechanism is known as active mineralization, in which the mineral is formed involving diverse bacterial metabolic pathways (e.g., ureolytic/urea hydrolysis, denitrification, sulfate reduction, iron reduction, and anaerobic sulfide oxidation) [21,54,59,78].

In bacterial-induced mineral precipitation, several bacteria have the ability to participate such as *Cyanobacteria, sulfate-reducing bacteria, Bacillus, Myxococcus, Halo bacteria, Pseudomonas*, and *Sporosarcina* [81]. It has been proven that *Sporosarcina pasteurii* (*S. pasteurii*) causes mineralization through the biologically induced mineralization mechanism [6,7]. *S. pasteurii* is a non-pathogenic, ureolytic, aerobic, and alkaliphilic bacteria with a high specific surface area of cells, low aggregation between cells, and the capacity to utilize urea as an energy and nitrogen source in metabolism, all of which contribute to their tremendous ability to adapt in the environment [87]. In the work of Hatayama [33]; $MnCO_3$ induced aerobically by calcite-forming bacteria was studied using *E. adhaerens, M. testaceum, Ps. protegens, and R. texasensis* on agar medium at 28 °C for over seven days. They found that $MnCO_3$ occurred extracellularly, and the increased pH would generate carbonate ions to form $MnCO_3$ with Mn ions. Furthermore Rivadeneyra et al. [67], formed mineral precipitates of rhodochrosite and dolomites using *Halomonas maura* in low or high $MnCl_2$ concentration. Their result showed that *H. maura* plays an essential role in biomineralization, in which the absence of bacteria has resulted in no precipitation that occurs with heat-killed cells. This observation could confirm that *H. Maura* acts as an inert nucleation site for precipitation and has an active role in other halophilic and non-halophilic microorganisms, as reported by Cailleau et al. [12] and Sanchez-Roman et al. [68]. Thus, the bacteria had a large effect in these studies, but geochemical conditions and manganese concentrations were also particularly influential.

Numerous methods have been reported to remove heavy metals from the environment, including electrolytic deposition [61], electrochemical [85], ion exchange [64], chemical oxidation-reduction [90], electro-dialysis [39], reverse osmosis [39], membrane separation [70], and solar water evaporation [89]. These methods are highly effective but have high operation costs and energy consumption and are often linked to the production of toxic sludge [23,76]. The adsorption process is the most commonly used and preferred method for heavy metal removal. This process occurs when the adsorbate is bound to the surface or inside the adsorbent [27]. The adsorption process uses synthetic or natural adsorbents and is simple, cost-effective, and versatile [64,76]. However, recent studies have pointed out a concern in the development of adsorbent material synthesis, which needs to be high-efficiency, with high surface area and porosity, but also with reduced synthesis time and cost of adsorbents [34]. Some prominent adsorbents, such as carbon, exhibit great ability for adsorption capacity due to their large surface area and ease of modification with other chemicals. However, the manufacturing process is high-cost, activated carbon is challenging to dispose of, and the regeneration process is time-consuming [57,84].

The present study aims at the development of $MnCO_3$ precipitate through biologically-induced mineralization mechanism employing *Sporosarcina pasteurii* as a catalyzing agent. Factor affecting precipitation, such as concentration of $MnCl_2$ has been

evaluated and tried to identify the best adsorbent based upon characterization. Adsorption potential of heavy metal of the prepared adsorbent has been investigated. In addition, the mechanism, involved in the mineralization process has also been highlighted in this work.

2. Experimental section

2.1. Chemical and reagents

A non-pathogenic bacteria *S. pasteurii* was inoculated in Tris-YE medium to grow the bacteria, was reported by Stocks-Fischer et al. [73] and Ghosh et al. [31]. The following chemical reagents was purchased from Sigma-Aldrich as $(NH_4)_2SO_4$, Yeast extract, $MnCl_2{\cdot}4H_2O$, Tris-Base, Urea and ethanol.

2.2. Bacteria growth conditions

Sporosarciana pasteurii DSM 33 was inoculated in Tris-YE medium [31,73], containing 0.13 M Tris-Base, $(NH_4)_2SO_4$ 10 g, and yeast extract 20 g, in 1 liter of distilled water at pH 8.5. The culture medium was shaken at 160 rpm under incubation at 30 °C for 48 h. The optical density (OD) of the *S. pasteurii* solution reached about 1.4, as recorded by evaluating the bacterial broth using UV–Visible spectrophotometry (Prema Pro-739) at a wavelength of 600 nm [6,7].

2.3. Synthesis of BISMCP

The details of synthesis conditions are listed in Table 1 for samples 1 to 9 (MCP-1 to MCP-9) [6].

Based on Atla et al. [6]; this study synthesizes BISMCP through biologically induced mineralization. The $MnCl_2{\cdot}4H_2O$ at various concentrations (i.e., 0.01 M; 0.1 M; 1 M), together with urea 1.0 M (control), were mixed in different volumes of Milli-Q water and *S. pasteurii* (with an OD of about 1.4). The solutions were put into screw-capped tubes at a total volume of 30 ml. The tubes were kept in an incubated shaker at 160 rpm at 30 °C for 24 h. The BISMCP was washed several times with Milli-Q water and ethanol. The samples were separated by centrifugation at 10,000 rpm at 15 °C for 3.5 min and dried in an air precision oven for 48 h at 50 °C. The results were synthesized as a white-yellowish precipitate.

2.4. Characterization of BISMCP

The powder XRD patterns were collected on a Bruker AXS D8 diffractometer (Bruker, Germany) at 40 kV and 40 mA operating conditions using Cu-Kα radiation ($\lambda = 0.154$ nm). The scanning rate was 2°/min with a diffraction angle (2θ) ranging between 10 and 80°. The functional groups of these materials were determined using FTIR spectra and acquired in the wavenumber range 4000–500 cm^{-1} on Jasco FT/IR-430 Plus spectrometer (Jasco, Japan) with the KBr pellet method. The morphology of the BISMCP was assessed by Field Emission Scanning Electron Microscopy (FESEM Hitachi S-4800) at various magnifications, operated at 15.0 kV. The energy dispersive X-ray spectroscopy (EDX) analysis was demonstrated on the sample using the silicon detector of the FESEM for elemental analysis and mapping. The pore size, pore volume, and specific surface area (SSA) analysis was performed using the Brunauer, Emmett, and Teller method with a surface area analyzer instrument (BET, Micromeritics, ASAP 2020 PLUS, USA) in the presence of liquid nitrogen at 77 K.

2.5. The potential application of BISMCP in the adsorption study

In the present study, 0.025 g of BISMCP was added to 20 ml of 5 ppm ICP multi-element standard solution XIII to determine the adsorption removal efficiency of heavy metals. The concentration of 5 ppm heavy metals were diluted from 100 ppm. of liquid solution of ICP multi-element standard solution XIII. The pH of the suspension was maintained at about six due to $pH_{PZC} = 5.5$. All samples were shaken for 48 h at room temperature to reach adsorption equilibrium. Then, the samples were filtered using a 0.2 μm glass syringe filter to remove the BISMCP sorbents and obtain the filtrate solutions. The filtered samples were taken from the screw-capped glass tubes for subsequent analysis and measured using Inductively Coupled Plasma-Optical Emission Spectroscopy (ICP-OES) (Agilent 5100 series).

The removal efficiency of heavy metals can be calculated according to Eq. (1) [25]:

Table 1
Details of synthesis composition to obtain BISMCP.

Milli-Q (ml)	30	20	10	0
S. pasteurii (ml)	0	10	20	30
$MnCl_2$ (0.01 M)	–	+ (MCP-1)[a]	+ (MCP-2)[a]	+ (MCP-3)[a]
$MnCl_2$ (0.1 M)	–	+ (MCP-4)	+ (MCP-5)	+ (MCP-6)
$MnCl_2$ (1 M)	–	+ (MCP-7)	+ (MCP-8)	+ (MCP-9)

[a] Tltc: too little to count.

$$\text{Removal Efficiency } (\%) = \frac{C_0 - C_e}{C_0} \times 100\% \quad (1)$$

where *Removal Efficiency (%)* is the heavy metal removal efficiency, shown as a percentage (%); C_0 is the initial heavy metal concentration and C_e is the equilibrium heavy metal concentration, both in mg/L [1,42].

3. Results and discussion

Biologically induced mineralization can result from metabolite excretion, such as urea hydrolysis, with cell surfaces and outer layers often acting as nucleation sites, substrates, or matrices for subsequent mineral precipitation [52]. *S. pasteurii* is a rapid-growing ureolytic bacteria and was cultured on media modified with different concentrations of $MnCl_2$ and bacterial volume to form a mineralization precipitate. As a result, the bacteria made the environment more alkaline (pH increased). The increased pH subsequently supported the equilibrium transition from bicarbonate to carbonate ions [73]. For media with a concentration of 0.1 M of $MnCl_2$ and a volume of bacteria of 10, 20, and 30 ml, the pH was increased from 8.6 to 10.7. Meanwhile, with the higher concentration of $MnCl_2$ (1 M), even with the volume of bacteria at 10, 20, and 30 ml, the pH was decreased, becoming 5.1, as predicted based on the high concentration of Mn^{2+} [52]. Table 1 shows that BISMCP was not produced without induction by bacteria (*S. pasteurii*) [6,7,33]. Most combinations of the $MnCl_2$ concentration and the volume of *S. pasteurii* yielded mineralization of BISMCP. However, for the lowest concentration of $MnCl_2$, 0.01 M (MCP-1, MCP-2, MCP-3), the precipitate was produced less than 0.1 g per sample and thus was not considered significantly. Therefore, characterization will only focus on $MnCl_2$ at a concentration of 0.1 M (MCP-4, MCP-5, MCP-6) and $MnCl_2$ at 1 M (MCP-7, MCP-8, MCP-9), as discussed in below. The characterizations included XRD, FTIR, FESEM-EDX, and BET analysis to know the physicochemical properties of BISMCP.

3.1. Structural and phase analysis of BISMCP by XRD

The phase crystalline and structural characteristics of BISMCP were obtained before the calcination process (Fig. 1), using a wide-angle XRD spectrum at a scan rate of 2°/min in 0.02-degree increments. The XRD patterns of the samples MCP-4 to MCP-9 reveal strong peaks, indicating that the materials are highly crystalline [38,58,61,74]. All sample patterns (Fig. 1) fitted well with JCPDS No. 44–1472, crystalline $MnCO_3$; which is comparable with the previous results [58,74]. Based on JCPDS No. 44–1472, the BISMCP had a rhombohedral-centered phase with the space group $R\underline{3}c$, commonly known as a property of the calcite group (ACO_3). As Hussain [33] mentioned, $MnCO_3$ (rhodochrosite) could be categorized as one of the calcite-structure metal carbonates. The ten diffraction peaks that appeared in BISMCP were indexed at 24.198°; 31.271°; 37.505°; 41.287°; 45.068°; 49.586°; 51.548°; 59.969°; 63.751°; and 67.389°, corresponding to the diffraction planes of (0 1 2); (1 0 4); (1 1 0); (1 1 3); (2 0 2); (0 2 4); (0 1 8); (1 2 2); (2 1 4); and (3 0 0) for crystalline $MnCO_3$ (rhodochrosite), which were indexed to the hexagonal system of the crystal structure. These results indicated that the particles obtained were rhodochrosite or $MnCO_3$ material, which was comparable with the results of $MnCO_3$ material synthesized in previous works [3,14,32,60,60].

3.2. Functional groups of BISMCP

The functional group of biologically-induced synthetic $MnCO_3$ precipitate (BISMCP) was determined by FTIR spectroscopy in the range of 4000–500 cm^{-1} (Fig. 2).

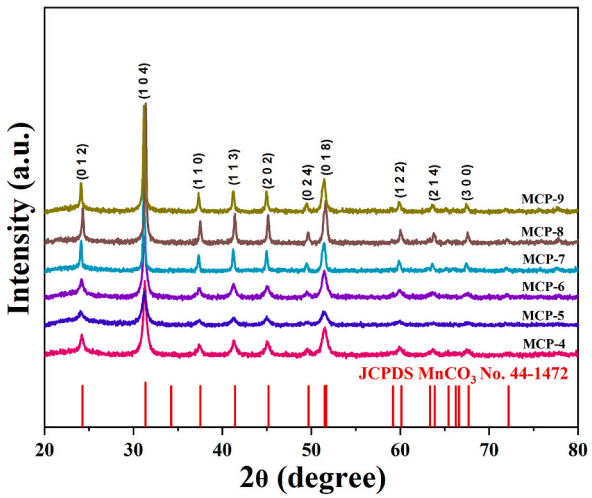

Fig. 1. The diffraction patterns of synthesized BISMCP (MCP-4 to MCP-9) in different concentration of $MnCl_2$ and volume of *S. pasteurii*.

The KnowItAll software can identify numerous functional groups in synthesized materials [56]. This software demonstrated a typical FT-IR spectrum of biologically-induced mineralization of $MnCO_3$, as shown in Fig. 2 The spectral peaks in MCP-4 to MCP-9 centered at 1420.90 cm^{-1}, 865.67 cm^{-1}, and 717.91 cm^{-1} are related to C═O binding and are known to be the typical peaks of rhodochrosite material or $MnCO_3$ [29,41,50,80,86]. The broader peak at 3452.24 cm^{-1} correlated to O–H binding and N–H binding, which were related to the characteristics of the hydroxyl and amino groups and could be attributed to sugars, carboxylic acids, nucleic acids, or amino acids [26]. The adsorption band at 2974.75 cm^{-1} with the intensity ratios of CH_2 asymmetric and symmetric stretching of CH_3 bands at 2494.58 cm^{-1} could indicate the occurrence of long-chain hydrocarbon derivatives, such as lipids and acid esters/-sugar alcohol [3].

The absorption bands at 1641.79 cm^{-1} in all samples MCP-4 to MCP-9 indeed confirm the existence of C═O binding and strong stretching of CO_3^{2-} in Amide I [3,80]. Moreover, the weak adsorption band at 1081.34 cm^{-1} is related to symmetric C–O stretching in the urethane group [3,37,61,79,83]. In addition, the bands at 805.22 cm^{-1} are occupied by the phosphate group of the P–CH_3 binding and the strong stretching silicon group of the Si–O binding. The peak at 717.91 cm^{-1} demonstrated the presence of phosphate group and its coordination in the P═S binding with stretching vibration. Therefore, these FT-IR results in MCP-4 to MCP-9 suggest that the functional groups of N–H in amine (protein), C═O in amide I, and C–O in urethane (carbamic acid) could be due to the formation of BISMCP; it is comparable with the previous results of Enyedi et al. [26]. Since all samples (MCP-4 to MCP-9) contained the CO_3^{2-} band and FT-IR bands matched to the previous study [3,26,87,79]; the functional groups in this study can be likewise identified as rhodochrosite mineral or $MnCO_3$ material [3,26,79,86].

3.3. Morphology and element signature of BISMCP

The low-magnification FESEM images shown in Fig. 3 (a-c) clearly show that the BISMCP particles were a spherical-like-aggregate shape. The particle size of BISMCP was on the micro-scale, about 3–8 μm (diameter). Moreover, in Fig. 3 (d-f), the BISMCP particles resemble aggregated spheres. This morphological condition could be related to the effect of different concentrations of $MnCl_2$ (0.1 M and 1 M) [46]. In contrast to the results of Hatayama [33]; the different types of manganese carbonate precipitation induced by diverse strains of calcite-forming bacteria in agar media were reported to have well-organized spherical shapes and a mean particle size of about 6–10 μm, which was bigger than this study. The precipitation material of BISMCP was analyzed by EDX for the specific analysis of elemental signature. The EDX results revealed the existence of manganese (Mn), carbon (C), and oxygen (O) elements (Fig. 3a–f), which confirmed the peak phase formation of $MnCO_3$ in BISMCP [40]. EDX showed that the Mn content (Wt.%) in the residues of MCP-4, MCP-5, MCP-6, MCP-7, MCP-8, and MCP-9 were 14.58%, 26.66%, 39.17%, 0.22%, 0.75%, and 12.54%, respectively. These results showed that various concentrations of $MnCl_2$ (0.1 M and 1 M) and different volumes of bacteria (10, 20, and 30 ml) affected the Mn content. Moreover, the Mn content in MCP-6 was higher than in the other samples, and this result is consistent with the specific surface area of BET characterizations.

3.4. Specific surface area, pore size, and pore volume of BISMCP

To determine the specific surface area and porosity structure, analysis by N_2 adsorption/desorption isotherms and BJH pore size distribution plots of the samples MCP-4 to MCP-9 were obtained as shown in Fig. 4 (a, b, and c) and summarized in Table 2. Based on the International Union of Pure and Applied Chemistry (IUPAC) classification, all six kinds of materials were type IV isotherms, which indicated highly uniform cylindrical pores appeared (Fig. 4a and b) [46]. Fig. 4c shows that most of the pores are distributed between 1

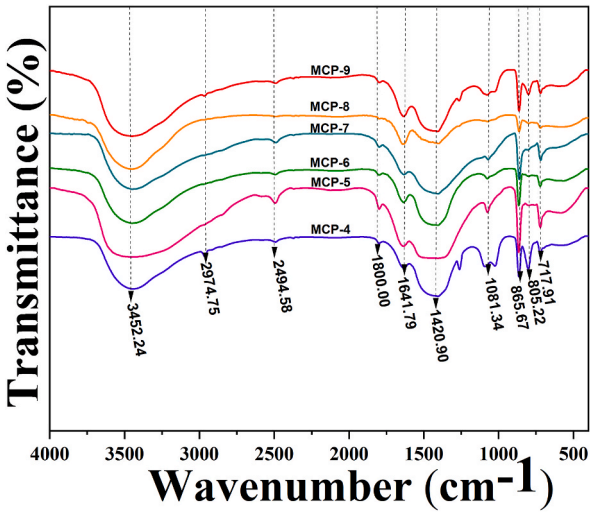

Fig. 2. The FTIR results of BISMCP in different concentrations of $MnCl_2$ and volumes of *S. pasteurii* (MCP-4 to MCP-9).

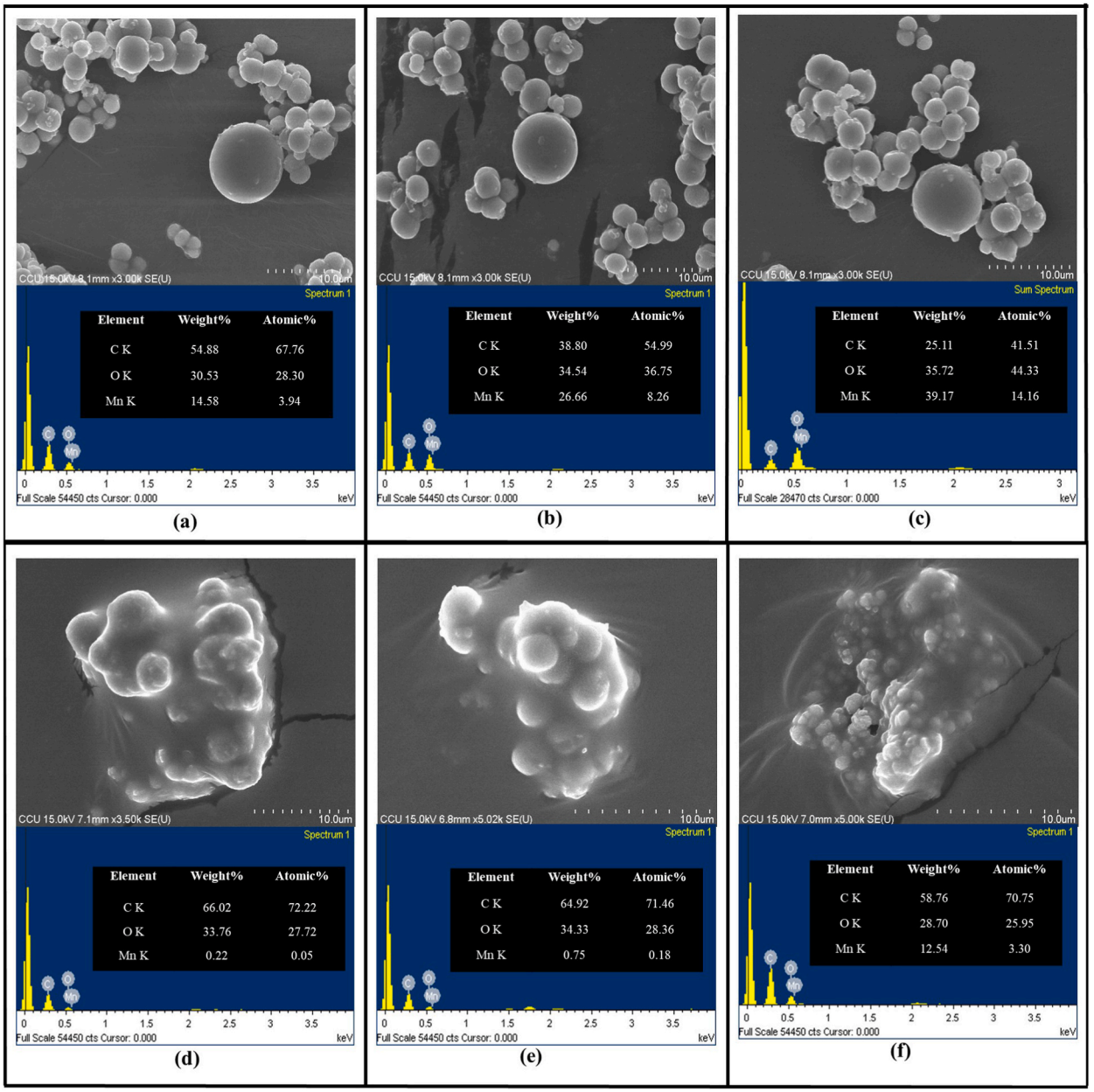

Fig. 3. FESEM and EDX of synthesized BISMCP in different concentrations of $MnCl_2$ (0.1 and 1 M) and volumes of *S. pasteurii* (10, 20, and 30 ml) MCP-4 (a), MCP-5 (b), MCP-6 (c), MCP-7 (d), MCP-8 (e), and MCP-9 (f).

and 10 nm, which are mesopores, comparable to the work of Jia et al. [36] and Kozawa [45]. From Table 2, the specific surface area and pore volume increased in the MCP-4, MCP-5, and MCP-6 (concentration of $MnCl_2$ 0.1 M), which confirmed the increase in the bacterial volume of 10, 20, and 30 ml could affect. However, the specific surface area and pore volume in the MCP-7, MCP-8, and MCP-9 (concentration of $MnCl_2$ 1 M) were not high, which could indicate that the concentration of $MnCl_2$ also affected the surface area. The average pore size of MCP-6 (9.76 nm) is quite large, which is suitable for adsorption studies [47]. Xie et al. [82] also noted that the larger pore volume was linearly associated with a larger specific surface area.

The specific surface area of the adsorbent is one of the critical parameters for enhancing removal efficiency [54]. A larger specific surface area was correlated with excellent performance of the adsorbent [51,66]. The BET results show that the unique characteristics of MCP-6, such as the higher specific surface area (BET = 109.01 m^2/g, and Langmuir = 171.64 m^2/g), smaller pore size (9.76 nm), and larger pore volume (0.178 cm^3/g), should give it a higher removal efficiency for metal ions than the other samples.

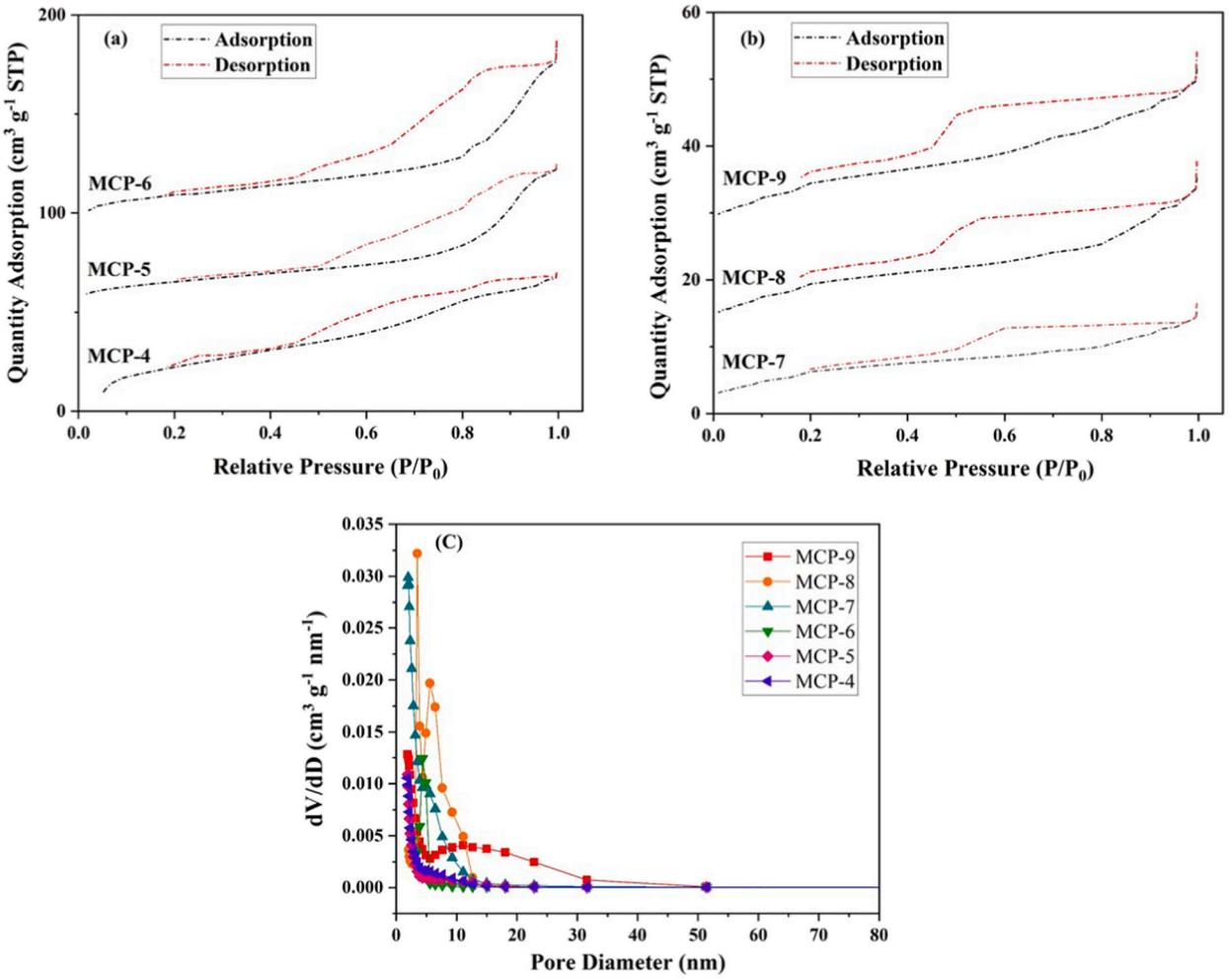

Fig. 4. The N2 adsorption/desorption isotherms of MCP-4, MCP-5, MCP-6 materials (a), MCP-7, MCP-8, MCP-9 materials (b), and the BJH pore size distribution of MCP-4 to MCP-9 (c).

Table 2
The specific surface area (SSA), pore size, and pore volume of BISMCP. (MCP-4 to MCP-9).

Samples	Specific Surface Area (m^2/g)		Pore Size (nm)	Pore Volume (cm^3/g)
	BET	Langmuir		
MCP-4	65.49	96.76	8.13	0.116
MCP-5	78.87	117.60	8.52	0.152
MCP-6	109.01	171.64	9.76	0.178
MCP-7	30.37	43.99	4.62	0.027
MCP-8	40.67	58.42	5.14	0.041
MCP-9	42.23	61.95	5.41	0.044

3.5. The preliminary result of the adsorption study on application of BISMCP

To understand possible future applications of BISMCP, we applied these materials in a preliminary study on the adsorption of heavy metals. This preliminary study aims to know which kinds of heavy metals can be removed using BISMCP and, of the various concentrations of MCP-4 to MCP-9. In this study, we investigated the removal efficiency of BISMCP that analyzed from Eq. (1) in removing heavy metal ions from an aqueous solution using 0.025 g of BISMCP in a 20 ml solution of 5 ppm ICP-OES multi-element standard solution XIII. It was found that BISMCP was able to remove As, Cr, Cu, Cd, Ni, and Zn from the aqueous solution, as shown in Fig. 5 and summarized in Table 3.

From Fig. 5 and Table 3 and it can be seen that BISMCP removed As, Cr, Cu, Cd, Ni, and Zn from the aqueous solution. The removal

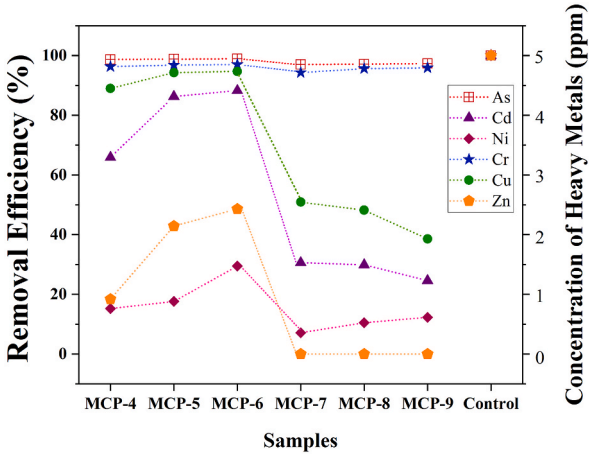

Fig. 5. The removal efficiency of numerous heavy metals in potential application of MCP-4 to MCP-9 and control (only heavy metals).

Table 3
The removal efficiency of BISMCP (MCP-4 to MCP-9) on total As, Cr, Cd, Cu, Ni, and Zn.

Samples	As (%)	Cr (%)	Cd (%)	Cu (%)	Ni (%)	Zn (%)
Control	100 (5 ppm)	100 (5 ppm)	100 (5 ppm)	100 (5 ppm)	100 (5 ppm)	100 (5 ppm)
MCP-4	98.7	96.3	65.9	89.0	15.2	18.4
MCP-5	98.8	96.8	86.3	94.3	17.6	42.9
MCP-6	98.9	97.0	88.3	94.7	29.5	48.6
MCP-7	97.0	94.3	30.6	50.9	7.1	0.0[a]
MCP-8	97.1	95.6	29.9	48.2	10.5	0.0[a]
MCP-9	97.3	95.9	24.6	38.6	12.3	0.0[a]

[a] No removal efficiency results.

efficiency of total As on the surface of MCP-4 to MCP-9 sorbents was over 97.0%. Moreover, the removal percentages of total Cr for six kinds of sorbents exhibited a high efficiency, above 94.0%. The highest removal efficiencies for both total As and Cr were about 98.9% and 97.0%, respectively in MCP-6 sorbent. However, the results of removal efficiencies in total Cu and Cd fluctuated between the six kinds of MCP sorbents. It can be shown that there was a similar trend between the sequence of MCP-4, MCP-5, and MCP-6 (concentration of $MnCl_2$ 0.1 M) and MCP-7, MCP-8, and MCP-9 (concentration of $MnCl_2$ 1 M). The trend on both total Cu and Cd removal can be written as the efficiency of MCP-6 > MCP-5 > MCP-4 > MCP-7 > MCP-8 > MCP-9, as shown in Table 3. The BISMCP also showed some ability to remove Ni, but the efficiency was below 30%. Even for the removal of Zn, only MCP-6 and MCP-5 showed moderate ability, while the efficiency of MCP-4 dramatically decreased to 18.4% and MCP-7, MCP-8, and MCP-9 sorbents showed no ability to remove Zn.

This condition of efficiency results from the surface of the six kinds of BISMCP sorbents being affected by the pH adjustment [28]. This can directly influence the surface charge of material (adsorbent), while also affecting on ionic state distribution of heavy metals (adsorbate) in the solution [16]. In this adsorption study, the pH_{PZC} of BISMCP was observed 5.5 (Fig. 6), confirming the result of a previous study [13]. The pH of 6.0 was chosen for all adsorption experiments since the surface of BISMCP becomes negatively charged at a pH higher than the pH_{PZC} of 5.5, and this enhances the adsorption of the positively charged metal ions through electrostatic forces

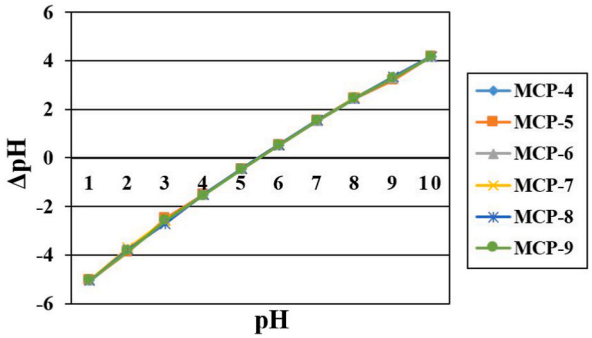

Fig. 6. The point of zero charges (pH_{PZC}) of MCP-4 to MCP-9.

of attraction and ion exchange [2,22,24].

In summary, the removal efficiency of As and Cr was the highest, with Cu, Ni, and Zn lower, which could indicate that As and Cr are more favorable for adsorption on the surface of MCP-4 to MCP-9 sorbents. One parameter that determines the removal efficiency is interaction between different heavy metal ions [54]. It seems likely that the occupancy of adsorption sites by As, and Cr may have prevented the adsorption of Cd, Cu, Ni, and Zn. The stronger binding (greater affinity) of As and Cr adsorption with six kinds of BISMCP sorbents compared to Cd, Cu, Ni, and Zn could be attributed to higher electronegativity, lower hydration energy, and a smaller hydrated radius [15,88].

The electronegativities of As, Cr, Cd, Cu, Ni, and Zn are 2.6, 1.66, 1.7, 1.9, 1.91, and 1.6, respectively [5,30,48,75,88]). The increases in electronegativity are linear with the increases of the electronic attraction to counter-ions [88]. Moreover, the hydration energies of Cr, Cd, Cu, Ni, and Zn are −1904, −1807, −2100, −2105, and −2046 kJ/mol, respectively [72,88]. While, the hydration energy for As, estimated at around −2608 kJ/mol and it is the lowest than others, which suggests that ions with lower hydration energy are more likely to be absorbed into the surface of the adsorbent [14,20,88]. The hydrated radius of Cr, Cd, Cu, Ni, and Zn is 0.413, 0.426, 0.419, 0.404, and 0.430 nm, respectively [77,88]. The hydrated radius of various groups of As is about 0.200–0.300, and the smallest hydrated radius will have a more significant electrostatic attraction [4,20,62]. Thus, in this study, the efficiency of As removal is higher than others because As has higher electronegativity, lower hydration energy, and a smaller hydrated radius, all of which makes As more favorable for adsorption compared to other metal ions.

As expected, the MCP-6 sorbent showed a higher removal efficiency for heavy metal than other sorbents. This result indicated that larger specific surface area and pore volume improve removal efficiency [63]. The BET analysis also determined that all BISMCP sorbents are mesopores materials, confirming the work of Liu et al. [53], in which the porous surface of the material (Mn composite oxide) enabled a large specific surface area and a large number of active sites. Thus, it could be suggested that the six MCP sorbents have good performance, especially for As and Cr removal, due to this porous condition.

The composition modification in the synthesis of BISMCP sorbents (MCP-4 to MCP-9) with various concentrations of $MnCl_2$ (0.1 M and 1 M) and different volumes of bacteria (10, 20, and 30 ml) indicated that the concentrations chosen affected not only the existence of Mn by EDX analysis, the specific surface area, and pore volume, but also the removal efficiency of total As, Cr, Cd, Cu, Ni, and Zn. This indicates that concentration modification enhanced the specific surface area and the efficiency of the adsorption of heavy metal ions [54].

3.6. The predicted mechanism of formation BISMCP

Based on the characterization analysis presented above, the predicted mechanism of biologically-induced synthetic $MnCO_3$ precipitate (BISMCP) is proposed in Fig. 7. The BISMCP material was produced by biologically induced mineralization through the urea hydrolysis process. Urea hydrolysis is an irreversible reaction in which urea reacts with water to generate ammonium and carbonate. However, chemical (un-catalyzed) hydrolysis of urea is a prolonged process and requires the urease enzyme to catalyze the reaction [8,44,78]. Therefore, *S. pasteurii* could produce urease enzymes to catalyze the hydrolysis of urea increase the rate of the reaction process. Thus, once water and urea react with the active site of the urease enzyme, this could produce carbonate and ammonium faster in the bacteria (the intracellular process). Furthermore, the appearance of $MnCl_2$ could attract the positive-charged ions Mn^{2+} (cations) to the negatively charged *S. pasteurii* cell wall (anions). The dissolved carbonate from the urea hydrolysis process, together with $MnCl_2$ present in the high alkaline environment around the cells (the extracellular process), gets converted into BISMCP and precipitated material into a solid form [11,18,44,73]. Interestingly, *S. pasteurii* can thrive in manganese dichloride salt environments because of its alkaliphilic and halophilic characteristics [19,49,55].

4. Conclusions

BISMCP material was successfully produced using a biologically induced mineralization method through the metabolic activity of *S. pasteurii*. The XRD results confirmed that MCP-4 to MCP-9 have the characteristics of rhodochrosite, with a rhombohedral-centered phase. Moreover, the FTIR software analysis indicated the appearance of the functional groups of N–H in amine, C═O in amide I, and C–O in urethane. The BISMCP showed a spherical-like-aggregate shape with a particle size of 3–8 μm. Meanwhile, EDX results confirmed the appearance of Mn, C, and O elements, with MCP-6 having the highest proportion of Mn content (Wt.%) at 39.17%. This result is consistent with the BET analysis, which puts MCP-6 as the highest at 109.01 m^2/g. Both EDX and BET results indicate that the relative concentration of $MnCl_2$ (0.1 and 1 M) and bacteria (10, 20, and 30 ml) affect BISMCP formation. The adsorption efficiency showed that compared to other sorbents, MCP-6 removed more As, Cr, Cd, Cu, Ni, and Zn, reaching 98.9%, 97.0%, and 94.6% for As, Cr, and Cu removal, respectively. This suggests that materials with a high specific surface area can perform well in removing heavy metals. Finally, it is concluded that MCP-6 is the best adsorbent compared to other BISMCP materials. Further adsorption studies specifically will focus on As removal due to its high efficiency of 98.9%.

Author contribution statement

Anggraeni Kumala Dewi: Performed the experiments; Analyzed and interpreted the data; Wrote the paper.

Raju Kumar Sharma, Uttara Sukul and Koyeli Das: Conceived and designed the experiments; Wrote the paper.

Pin-Yun Lin, Yi-Hsun Huang, Chung Ming Lu, Cheng-Kang Lu, Tsung-Hsien Chen: Contributed reagents, materials, analysis tools or data.

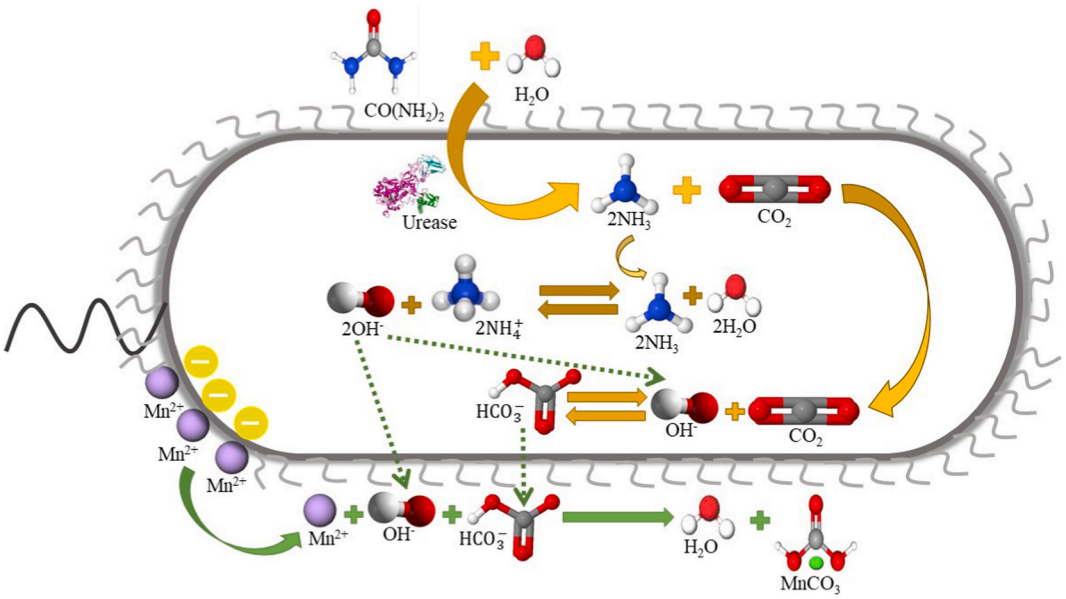

Fig. 7. Predicted mechanism of BISMCP mineralization by biologically induced mineralization.

Chien-Yen Chen: Conceived and designed the experiments.

Funding statement

This research did not receive any specific grant from funding agencies in the public, commercial, or not-for-profit sectors.

Data availability statement

Data will be made available on request.

Declaration of competing interest

The authors declare that they have no known competing financial interests or personal relationships that could have appeared to influence the work reported in this paper.

Acknowledgement

The authors would like to thank the Ministry of Science and Technology (Taiwan) for financial support (MOST 109-2811-M-194-502; MOST 108-2811-M-194-510). The authors would also like to thank the National Science and Technology Council (Taiwan) for financial support (NSTC 111-2124-M-194-001; NSTC 111-2116-M-194-011). This research was funded in part by Ditmanson Medical Foundation Chiayi Christian Hospital (CYCH-CCU-2022-12). Startup Value Creation Program (SVCP), 112-EC-17-A-08-S6-017. This research was received the Award for the Ninth Environmental Protection of ASE Foundation for Environmental Protection and Sustainability.

References

[1] M.K. Ahmed, S.F. Mansour, R. Ramadan, M. Afifi, M.S. Mostafa, S.I. El-dek, V. Uskokovic, Tuning the composition of new brushite/vivianite mixed systems for superior heavy metal removal efficiency from contaminated waters, J. Water Process Eng. 34 (2020), 101090, https://doi.org/10.1016/j.jwpe.2019.101090. ARTN 101090.

[2] K.G. Akpomie, F.A. Dawodu, K.O. Adebowale, Mechanism on the sorption of heavy metals from binary-solution by a low cost montmorillonite and its desorption potential, Alex. Eng. J. 54 (2015) 757–767.

[3] S. Ali, Y. Iqbal, K.H. Shah, M. Fahad, Synthesis and kinetic modeling of manganese carbonate precipitated from manganese sulfate solution, Chem. Eng. Commun. 209 (2022) 96–107.

[4] M. Aliaskari, A.I. Schafer, Nitrate, arsenic and fluoride removal by electrodialysis from brackish groundwater, Water Res. 190 (2021), 116683, https://doi.org/10.1016/j.watres.2020.116683.

[5] A. Allred, A. Hensley Jr., Electronegativities of nitrogen, phosphorus, arsenic, antimony and bismuth, J. Inorg. Nucl. Chem. 17 (1961) 43–54.

[6] S.B. Atla, C.Y. Chen, C.W. Fu, T.C. Chien, A.C. Sun, C.F. Huang, C.J. Lo, T.C. Yang, Microbial induced synthesis of hollow cylinder and helical NiO micro/nanostructure, Mrs Communications 4 (2014) 121–127, https://doi.org/10.1557/mrc.2014.24.

[7] S.B. Atla, Y.J. Chen, H.W. Chiu, C.C. Chen, J.C. Shu, C.Y. Chen, Microbial induced synthesis of CeCO3OH and CeO2 hollow rods micro/nanostructure, Mater. Lett. 167 (2016) 238–241, https://doi.org/10.1016/j.matlet.2015.12.123.

[8] S. Benini, W.R. Rypniewski, K.S. Wilson, S. Miletti, S. Ciurli, S. Mangani, A new proposal for urease mechanism based on the crystal structures of the native and inhibited enzyme from Bacillus pasteurii: why urea hydrolysis costs two nickels, Structure 7 (1999) 205–216, https://doi.org/10.1016/S0969-2126(99)80026-4.

[9] M.A. Borowitzka, Morphological and cytological aspects of algal calcification, in: International Review of Cytology, Elsevier, 1982, pp. 127–162.

[10] A.L. Boskey, Biomineralization: an overview, Connect. Tissue Res. 44 (Suppl 1) (2003) 5–9.

[11] M.B. Burbank, T.J. Weaver, T.L. Green, B.C. Williams, R.L. Crawford, Precipitation of calcite by indigenous microorganisms to strengthen liquefiable soils, Geomicrobiol. J. 28 (2011) 301–312, https://doi.org/10.1080/01490451.2010.499929. Pii 938115271.

[12] G. Cailleau, O. Braissant, C. Dupraz, M. Aragno, E.P. Verrecchia, Biologically induced accumulations of CaCO3 in orthox soils of Biga, Ivory Coast, Catena 59 (2005) 1–17, https://doi.org/10.1016/j.catena.2004.06.002.

[13] L. Charlet, P. Wersin, W. Stumm, Surface charge of MnCO3and FeCO3, Geochem. Cosmochim. Acta 54 (1990) 2329–2336.

[14] B. Chen, Z.B. Zhao, F. Liu, S.C. Yang, Y.L. Zhao, L.X. Cheng, Aerobic and additive-free oxidative dehydrogenation of N-heterocycles over commercial MnCO3-derived manganese oxides, ChemistrySelect 5 (2020) 14387–14392, https://doi.org/10.1002/slct.202004179.

[15] M. Chen, S. Nong, Y. Zhao, M.S. Riaz, Y. Xiao, M.S. Molokeev, F. Huang, Renewable P-type zeolite for superior absorption of heavy metals: isotherms, kinetics, and mechanism, Sci. Total Environ. 726 (2020), 138535, https://doi.org/10.1016/j.scitotenv.2020.138535.

[16] K. Choi, S.Y. Lee, H. Kim, K.B. Lee, J.-W. Choi, K.-W. Jung, Mechanistic insights into the simultaneous removal of as (V) and Cr (VI) oxyanions by a novel hierarchical corolla-like MnO2-decorated porous magnetic biochar composite: a combined experimental and density functional theory study, Appl. Surf. Sci. 578 (2022), 151991.

[17] R. Crichton, Biomineralization. Biological Inorganic Chemistry: A New Introduction to Molecular Structure and Function, 3rd Edition, 2019, pp. 517–544, https://doi.org/10.1016/B978-0-12-811741-5.00019-9.

[18] W. De Muynck, N. De Belie, W. Verstraete, Microbial carbonate precipitation in construction materials: a review, Ecol. Eng. 36 (2010) 118–136.

[19] P. De Vos, Tenuibacillus, in: Bergey's Manual of Systematic Bacteriology, Springer, 2009, pp. 191–192.

[20] M.W.C. Dharma-Wardana, Chronic kidney disease of unknown etiology and the effect of multiple-ion interactions, Environ. Geochem. Health 40 (2018) 705–719, https://doi.org/10.1007/s10653-017-0017-4.

[21] M.R. Diaz, G.P. Eberli, Decoding the mechanism of formation in marine ooids: a review, Earth Sci. Rev. 190 (2019) 536–556, https://doi.org/10.1016/j.earscirev.2018.12.016.

[22] T.C. Egbosiuba, A.S. Abdulkareem, Highly efficient as-synthesized and oxidized multi-walled carbon nanotubes for copper (II) and zinc (II) ion adsorption in a batch and fixed-bed process, J. Mater. Res. Technol. 15 (2021) 2848–2872.

[23] T.C. Egbosiuba, A.S. Abdulkareem, A.S. Kovo, E.A. Afolabi, J.O. Tijani, M.T. Bankole, S. Bo, W.D. Roos, Adsorption of Cr (VI), Ni (II), Fe (II) and Cd (II) ions by KIAgNPs decorated MWCNTs in a batch and fixed bed process, Sci. Rep. 11 (2021) 1–20.

[24] T.C. Egbosiuba, A.S. Abdulkareem, A.S. Kovo, E.A. Afolabi, J.O. Tijani, W.D. Roos, Enhanced adsorption of as (V) and Mn (VII) from industrial wastewater using multi-walled carbon nanotubes and carboxylated multi-walled carbon nanotubes, Chemosphere 254 (2020), 126780.

[25] T.C. Egbosiuba, A.S. Abdulkareem, J.O. Tijani, J.I. Ani, V. Krikstolaityte, M. Srinivasan, A. Veksha, G. Lisak, Taguchi optimization design of diameter-controlled synthesis of multi walled carbon nanotubes for the adsorption of Pb (II) and Ni (II) from chemical industry wastewater, Chemosphere 266 (2021), 128937.

[26] N.T. Enyedi, J. Makk, L. Kotai, B. Berenyi, S. Klebert, Z. Sebestyen, Z. Molnar, A.K. Borsodi, S. Leel-Ossy, A. Demeny, P. Nemeth, Cave bacteria-induced amorphous calcium carbonate formation, Sci. Rep. 10 (2020) 8696, https://doi.org/10.1038/s41598-020-65667-w.

[27] A. Ewecharoen, P. Thiravetyan, E. Wendel, H. Bertagnolli, Nickel adsorption by sodium polyacrylate-grafted activated carbon, J. Hazard Mater. 171 (2009) 335–339, https://doi.org/10.1016/j.jhazmat.2009.06.008.

[28] L. Fang, L. Li, Z. Qu, H. Xu, J. Xu, N. Yan, A novel method for the sequential removal and separation of multiple heavy metals from wastewater, J. Hazard Mater. 342 (2018) 617–624, https://doi.org/10.1016/j.jhazmat.2017.08.072.

[29] T.E. Flores-Guia, L.F. Cano Salazar, A. Martínez-Luévanos, J. Claudio-Rizo, Manganese oxides: synthesis and application as adsorbents of heavy metal ions, Handbook Nanomat. Nanocomposit. Energy Environ. Applicat. (2021) 2409–2428.

[30] G. Genchi, G. Lauria, A. Catalano, A. Carocci, M.S. Sinicropi, The double face of metals: the intriguing case of chromium, Appl. Sci. 11 (2021) 638.

[31] T. Ghosh, S. Bhaduri, C. Montemagno, A. Kumar, Sporosarcina pasteurii can form nanoscale calcium carbonate crystals on cell surface, PLoS One 14 (2019), e0210339, https://doi.org/10.1371/journal.pone.0210339. ARTN e0210339.

[32] R.R. Hao, J. Wang, S.W. Yao, Y.C. Lan, D.S. Li, X.X. Feng, The 3D networked MnCO3-C composite as anode materials for lithium ion batteries, J. Electroanal. Chem. 877 (2020), 114655, https://doi.org/10.1016/j.jelechem.2020.114655. ARTN 114655.

[33] K. Hatayama, Manganese carbonate precipitation induced by calcite-forming bacteria, Geomicrobiol. J. 37 (2020) 603–609, https://doi.org/10.1080/01490451.2020.1743391.

[34] A. Hussain, S. Madan, R. Madan, Removal of Heavy Metals from Wastewater by Adsorption, Heavy Metals—Their Environmental Impacts and Mitigation, 2021.

[35] N. Jalilvand, A. Akhgar, H.A. Alikhani, H.A. Rahmani, F. Rejali, Removal of heavy metals zinc, lead, and cadmium by biomineralization of urease-producing bacteria isolated from Iranian mine calcareous soils, J. Soil Sci. Plant Nutr. 20 (2020) 206–219, https://doi.org/10.1007/s42729-019-00121-z.

[36] R. Jia, Z. Huang, C. Zhao, X. Liu, D. Wang, Z. Hui, M. Zuo, S. Shi, X. Xu, Ultrafast synthesis of single-phase Mn1− xCoxCO3/GO with enhanced electrochemical performance for lithium-ion batteries, Ionics 26 (2020) 4463–4471.

[37] W. Jiang, A. Saxena, B. Song, B.B. Ward, T.J. Beveridge, S.C.B. Myneni, Elucidation of functional groups on gram-positive and gram-negative bacterial surfaces using infrared spectroscopy, Langmuir 20 (2004) 11433–11442, https://doi.org/10.1021/la049043+.

[38] M. Jin, H. Yuan, B. Liu, J. Peng, L. Xu, D. Yang, Review of the distribution and detection methods of heavy metals in the environment, Anal. Methods 12 (2020) 5747–5766, https://doi.org/10.1039/d0ay01577f.

[39] J.-M.A. Juve, F.M. Christensen, Y. Wang, Z. Wei, Electrodialysis for metal removal and recovery: a review, Chem. Eng. J. (2022), 134857.

[40] M. Karuppaiah, R. Akilan, P. Sakthivel, S. Asaithambi, R. Shankar, R. Yuvakkumar, Y. Hayakawa, G. Ravi, Synthesis of self-assembled micro/nano structured manganese carbonate for high performance, long lifespan asymmetric supercapacitors and investigation of atomic-level intercalation properties of OH− ions via first principle calculation, J. Energy Storage 27 (2020), 101138.

[41] M. Khan, S.F. Adil, M.E. Assal, A.I. Alharthi, M.R. Shaik, M. Kuniyil, A. Al-Warthan, A. Khan, Z. Nawaz, H. Shaikh, M.R.H. Siddiqui, Solventless mechanochemical fabrication of ZnO-MnCO3/N-doped graphene nanocomposite: efficacious and recoverable catalyst for selective aerobic dehydrogenation of alcohols under alkali-free conditions, Catalysts 11 (2021) 760, https://doi.org/10.3390/catal11070760. ARTN 760.

[42] W.A. Khoso, N. Haleem, M.A. Baig, Y. Jamal, Synthesis, characterization and heavy metal removal efficiency of nickel ferrite nanoparticles (NFN's), Sci. Rep. 11 (2021) 3790, https://doi.org/10.1038/s41598-021-83363-1.

[43] T. Klaus, R. Joerger, E. Olsson, C.G. Granqvist, Silver-based crystalline nanoparticles, microbially fabricated, Proc. Natl. Acad. Sci. U. S. A. 96 (1999) 13611–13614, https://doi.org/10.1073/pnas.96.24.13611.

[44] C. Konstantinou, Y. Wang, G. Biscontin, K. Soga, The role of bacterial urease activity on the uniformity of carbonate precipitation profiles of bio-treated coarse sand specimens, Sci. Rep. 11 (2021) 6161, https://doi.org/10.1038/s41598-021-85712-6.

[45] T. Kozawa, Microstructural development of MnCO3 microsphere compacts through hydrothermal hot-pressing, J. Eur. Ceram. Soc. 42 (2022) 1530–1536, https://doi.org/10.1016/j.jeurceramsoc.2021.12.022.

[46] M. Kruk, M. Jaroniec, Gas adsorption characterization of ordered organic-inorganic nanocomposite materials, Chem. Mater. 13 (2001) 3169–3183, https://doi.org/10.1021/cm0101069.

[47] P.S. Kumar, L. Korving, K.J. Keesman, M.C.M. van Loosdrecht, G.J. Witkamp, Effect of pore size distribution and particle size of porous metal oxides on phosphate adsorption capacity and kinetics, Chem. Eng. J. 358 (2019) 160–169, https://doi.org/10.1016/j.cej.2018.09.202.

[48] M. Laing, The electronegativity of a metal and its E o: should they correlate? South Afr. J. Sci. 98 (2002) 573–580.

[49] F.M. Lapierre, J. Schmid, B. Ederer, N. Ihling, J. Buchs, R. Huber, Revealing nutritional requirements of MICP-relevant Sporosarcina pasteurii DSM33 for growth improvement in chemically defined and complex media, Sci. Rep. 10 (2020), 22448, https://doi.org/10.1038/s41598-020-79904-9.

[50] H.K. Lee, D. Sakemi, R. Selyanchyn, C.G. Lee, S.W. Lee, Titania nanocoating on MnCO3 microspheres via liquid-phase deposition for fabrication of template-assisted core-shell- and hollow-structured composites, ACS Appl. Mater. Interfaces 6 (2014) 57–64, https://doi.org/10.1021/am404052p.

[51] M. Li, S. Kuang, Y. Kang, H. Ma, J. Dong, Z. Guo, Recent advances in application of iron-manganese oxide nanomaterials for removal of heavy metals in the aquatic environment, Sci. Total Environ. 819 (2022), 153157, https://doi.org/10.1016/j.scitotenv.2022.153157.

[52] Q. Li, L. Csetenyi, G.M. Gadd, Biomineralization of metal carbonates by Neurospora crassa, Environ. Sci. Technol. 48 (2014) 14409–14416, https://doi.org/10.1021/es5042546.

[53] L. Liu, Q. Qiao, W. Tan, X. Sun, C. Liu, Z. Dang, G. Qiu, Arsenic detoxification by iron-manganese nodules under electrochemically controlled redox: mechanism and application, J. Hazard Mater. 403 (2021), 123912, https://doi.org/10.1016/j.jhazmat.2020.123912.

[54] M. Liu, S. Wang, M. Yang, X. Ning, Z. Nan, Experimental study on treatment of heavy metal-contaminated soil by manganese-oxidizing bacteria, Environ. Sci. Pollut. Res. Int. 29 (2022) 5526–5540, https://doi.org/10.1007/s11356-021-15475-0.

[55] L. Ma, A.P. Pang, Y. Luo, X. Lu, F. Lin, Beneficial factors for biomineralization by ureolytic bacterium Sporosarcina pasteurii, Microb. Cell Factories 19 (2020) 12, https://doi.org/10.1186/s12934-020-1281-z.

[56] J.P. Maity, S. Kar, C.M. Lin, C.Y. Chen, Y.F. Chang, J.S. Jean, T.R. Kulp, Identification and discrimination of bacteria using Fourier transform infrared spectroscopy, Spectrochim. Acta Mol. Biomol. Spectrosc. 116 (2013) 478–484, https://doi.org/10.1016/j.saa.2013.07.062.

[57] A. Mukherjee, J.A. Okolie, A. Abdelrasoul, C. Niu, A.K. Dalai, Review of post-combustion carbon dioxide capture technologies using activated carbon, J. Environ. Sci. 83 (2019) 46–63.

[58] S. Muralikrishna, B. Kishore, H. Nagabhushana, D. Suresh, S. Sharma, G. Nagaraju, One pot green synthesis of MnCO 3–rGO composite hybrid superstructure: application to lithium ion battery and biosensor, New J. Chem. 41 (2017) 12854–12865.

[59] R. Murugan, G.K. Suraishkumar, A. Mukherjee, N.K. Dhami, Influence of native ureolytic microbial community on biocementation potential of Sporosarcina pasteurii, Sci. Rep. 11 (2021), 20856, https://doi.org/10.1038/s41598-021-00315-5.

[60] K. Murugesan, S. Perumal, A. Sankaiya, K.B. Lankamsetty, G. Nagaraju, B. Karuppannan, Y. Rathinam, R. Ganesan, Defect induced in 3D-rhombohedral MnCO3 microcrystals by substitution of transition metals for aqueous and solid-state hybrid supercapacitors, ACS Sustain. Chem. Eng. 9 (2021) 1656–1668, https://doi.org/10.1021/acssuschemeng.0c07342.

[61] A.T. Ojedokun, O.S. Bello, Sequestering heavy metals from wastewater using cow dung, Water Resour. Ind. 13 (2016) 7–13.

[62] A.P. Padilla, H. Saitua, Performance of simultaneous arsenic, fluoride and alkalinity (bicarbonate) rejection by pilot-scale nanofiltration, Desalination 257 (2010) 16–21, https://doi.org/10.1016/j.desal.2010.03.022.

[63] L.M. Pandey, Surface engineering of nano-sorbents for the removal of heavy metals: interfacial aspects, J. Environ. Chem. Eng. 9 (2021), 104586, https://doi.org/10.1016/j.jece.2020.104586. ARTN 104586.

[64] N.A. Qasem, R.H. Mohammed, D.U. Lawal, Removal of heavy metal ions from wastewater: a comprehensive and critical review, Npj Clean Water 4 (2021) 1–15.

[65] W. Qin, C. yu Wang, Y. xuan Ma, M. juan Shen, J. Li, K. Jiao, F.R. Tay, L. na Niu, Correction to: microbe-mediated extracellular and intracellular mineralization, Environ. Indust. Biotechnol. Applicat. (Advanced Materials,(2020) 32 (22) (2022), 1907833, https://doi.org/10.1002/adma.201907833. Advanced Materials 34, 2109924.

[66] B.B. Qiu, X.D. Tao, H. Wang, W.K. Li, X. Ding, H.Q. Chu, Biochar as a low-cost adsorbent for aqueous heavy metal removal: a review, J. Anal. Appl. Pyrol. 155 (2021), 105081, https://doi.org/10.1016/j.jaap.2021.105081. ARTN 105081.

[67] A. Rivadeneyra, A. Gonzalez-Martinez, G.R. Portela, D.J. Martin-Ramos, J. Gonzalez-Lopez, M.A. Rivadeneyra, Biomineralisation of carbonate and sulphate by the halophilic bacterium Halomonas maura at different manganese concentrations, Extremophiles 21 (2017) 1049–1056, https://doi.org/10.1007/s00792-017-0965-8.

[68] M. Sanchez-Roman, M.A. Rivadeneyra, C. Vasconcelos, J.A. McKenzie, Biomineralization of carbonate and phosphate by moderately halophilic bacteria, FEMS Microbiol. Ecol. 61 (2007) 273–284, https://doi.org/10.1111/j.1574-6941.2007.00336.x.

[69] M. Sarikaya, Biomimetics: materials fabrication through biology, Proc. Natl. Acad. Sci. U.S.A. 96 (1999) 14183–14185, https://doi.org/10.1073/pnas.96.25.14183.

[70] R. Shrestha, S. Ban, S. Devkota, S. Sharma, R. Joshi, A.P. Tiwari, H.Y. Kim, M.K. Joshi, Technological trends in heavy metals removal from industrial wastewater: a review, J. Environ. Chem. Eng. 9 (2021), 105688.

[71] H. Skinner, A. Jahren, W. Schlesinger, Treatise on geochemistry, Biomineralization 8 (2003) 117–184.

[72] D.W. Smith, Ionic hydration enthalpies, J. Chem. Educ. 54 (1977) 540.

[73] S. Stocks-Fischer, J.K. Galinat, S.S. Bang, Microbiological precipitation of CaCO3, Soil Biol. Biochem. 31 (1999) 1563–1571, https://doi.org/10.1016/S0038-0717(99)00082-6.

[74] D.Y. Su, J. Wang, Z. Yang, S. Liu, J.P. Yang, S.W. Yao, X.X. Feng, Stability electrochemical performance of self-assembled hierarchical MnCO3/MWCNT nanocomposite as anode material for lithium-ion batteries, J. Solid State Electrochem. 22 (2018) 3485–3491, https://doi.org/10.1007/s10008-018-4020-1.

[75] A. Taub, C. Briant, Composition dependence of ductility in boron-doped, nickel-base L12 alloys, Acta Metall. 35 (1987) 1597–1603.

[76] A. Tripathi, M.R. Ranjan, Heavy metal removal from wastewater using low cost adsorbents, J. Biorem. Biodegrad. 6 (2015) 315.

[77] K. Usman, M.A. Al-Ghouti, M.H. Abu-Dieyeh, The assessment of cadmium, chromium, copper, and nickel tolerance and bioaccumulation by shrub plant Tetraena qataranse, Sci. Rep. 9 (2019) 5658, https://doi.org/10.1038/s41598-019-42029-9.

[78] L.B. Van Paassen, Ground Improvement by Microbially Induced Carbonate Precipitation, Delft University of Technology, Delft, 2009.

[79] H. Wang, X. Pan, Role of extracellular polymeric substances (EPS) from Pseudomonas putida strain MnB1 in dissolution of natural rhodochrosite, Biogeosci. Discuss. 11 (2014) 7273–7290.

[80] L. Wang, Y. Sun, S. Zeng, C. Cui, H. Li, S. Xu, H. Wang, Study on the morphology-controlled synthesis of MnCO 3 materials and their enhanced electrochemical performance for lithium ion batteries, CrystEngComm 18 (2016) 8072–8079.

[81] S. Wei, H. Cui, Z. Jiang, H. Liu, H. He, N. Fang, Biomineralization processes of calcite induced by bacteria isolated from marine sediments, Braz. J. Microbiol. 46 (2015) 455–464, https://doi.org/10.1590/S1517-838246220140533.

[82] X. Xie, C. Lu, R. Xu, X. Yang, L. Yan, C. Su, Arsenic removal by manganese-doped mesoporous iron oxides from groundwater: performance and mechanism, Sci. Total Environ. 806 (2022), 150615, https://doi.org/10.1016/j.scitotenv.2021.150615.

[83] H.Y. Xu, X.Y. Yu, Pressed gibbsite and calcite as a rhodochrosite imitation, Gems Gemol. 55 (2019) 406–415, https://doi.org/10.5741/Gems.55.3.406.

[84] M.A. Yahya, Z. Al-Qodah, C.Z. Ngah, Agricultural bio-waste materials as potential sustainable precursors used for activated carbon production: a review, Renew. Sustain. Energy Rev. 46 (2015) 218–235.

[85] L. Yang, W. Hu, Z. Chang, T. Liu, D. Fang, P. Shao, H. Shi, X. Luo, Electrochemical recovery and high value-added reutilization of heavy metal ions from wastewater: recent advances and future trends, Environ. Int. 152 (2021), 106512.

[86] H. Zhang, X. Pan, Q. Wu, J. Guo, C. Wang, H. Liu, Manganese carbonate nanoparticles-mediated mitochondrial dysfunction for enhanced sonodynamic therapy, in: 2. (Wiley Online Library), 2021, 20210010.

[87] J.H. Zhang, X.Z. Shi, X. Chen, X.F. Huo, Z. Yu, Microbial-induced carbonate precipitation: a review on influencing factors and applications, Adv. Civ. Eng. (2021), https://doi.org/10.1155/2021/9974027. Artn 9974027.

[88] D. Zhou, D.G. Kim, S.O. Ko, Heavy metal adsorption with biogenic manganese oxides generated by Pseudomonas putida strain MnB1, J. Ind. Eng. Chem. 24 (2015) 132–139, https://doi.org/10.1016/j.jiec.2014.09.020.

[89] X. Zhou, F. Zhao, P. Zhang, G. Yu, Solar water evaporation toward water purification and beyond, ACS Materials Letters 3 (2021) 1112–1129.

[90] W. Zuo, Y. Yu, H. Huang, Making waves: microbe-photocatalyst hybrids may provide new opportunities for treating heavy metal polluted wastewater, Water Res. 195 (2021), 116984.